Hindawi
International Journal of Energy Research
Volume 2023, Article ID 6016603, 10 pages
https://doi.org/10.1155/2023/6016603

Research Article

Comparative Study on Hydrogen Evolution Reaction of Various Cobalt-Selenide-Based Electrocatalysts

Ha Huu Do,[1] **Quyet Van Le**,[2] **Jin Hyuk Cho**,[2] **Sang Hyun Ahn**,[1] **and Soo Young Kim**[2]

[1]*School of Chemical Engineering and Materials Science, Chung-Ang University, 84 Heukseok-ro, Dongjak-gu, Seoul 06974, Republic of Korea*
[2]*Department of Materials Science and Engineering, Institute of Green Manufacturing Technology, Korea University, 145 Anam-ro, Seongbuk-gu, Seoul 02841, Republic of Korea*

Correspondence should be addressed to Sang Hyun Ahn; shahn@cau.ac.kr and Soo Young Kim; sooyoungkim@korea.ac.kr

Received 10 November 2022; Revised 14 December 2022; Accepted 19 December 2022; Published 3 February 2023

Academic Editor: Prakash Bhuyar

The growth of stable and efficient catalysts is vital for the electrochemical hydrogen evolution reaction (HER). Metal–organic frameworks (MOFs) have been recognized as ideal templates for fabricating efficient nanomaterial-based electrocatalysts for the HER. In this study, nitrogen-containing Co-MOF (ZIF-67), Co-MOF-74, and cobalt chloride salt were selenized to create various cobalt-selenide-based materials, i.e., cobalt selenide@nitrogen-doped carbon ($CoSe_2$@NC), $CoSe_2$@C, and $CoSe_2$, respectively. The core–shell structure of $CoSe_2$@NC originated from ZIF-67 exhibited better HER catalytic activity than those of $CoSe_2$@C and $CoSe_2$. $CoSe_2$@NC exhibited a low overvoltage of 184 mV at 10 mA cm^{-2} and a small Tafel slope of 58.4 mV dec^{-1}. In addition, this catalyst exhibited excellent durability while maintaining its performance after 12 h of testing. The high catalytic activity is ascribed to the integrated effect of the core–shell architecture, N-doped carbon, and large surface area, making protected active sites, high conductivity, and exposed active sites possible. The results demonstrate the efficiency of using MOFs as precursors for cobalt selenide fabrication and provide a potential synthetic strategy for noble-metal-free electrocatalysts for hydrogen production.

1. Introduction

The overuse of fossil fuels is undoubtedly taking a heavy toll on the environment owing to carbon emissions and chemical waste. Therefore, finding sustainable and environmentally friendly energy sources is important [1, 2]. The electrochemical hydrogen evolution reaction (HER) is a noncarbon pathway that produces hydrogen to replace fossil fuels [3–6]. However, the high-energy requirement for water splitting impedes hydrogen formation at a high flow rate. Traditionally, catalysts have been applied for water electrolysis to reduce the energy barrier and accelerate reaction kinetics [7–9]. Pt-based materials are promising catalysts for HER [10–12]. For example, Chen et al. prepared a ternary Pt-Ni-Co electrocatalyst with a very small overvoltage [13]. Shen et al. created trimetallic Pt-Cu-Ni nanograins embedded on carbon fiber as an outstanding cathode, which exhibits an excellent HER performance in both acidic and alkaline electrolytes [14]. However, they are expensive and unstable under reaction conditions. Thus, the development of nonprecious electrocatalysts with excellent activity and outstanding durability is vital for industrial applications [15–17].

Transition-metal selenides, such as $MoSe_2$, WSe_2, $CoSe_2$, and $NiSe_2$ [18–22], are Pt-free electrocatalysts with high performance for water dissociation, as proved in theoretical and experimental studies. Among these materials, $CoSe_2$ exhibits a remarkable performance and high stability in various solutions. However, the agglomeration of $CoSe_2$ nanograins, which usually occurs during the synthesis process, decreases

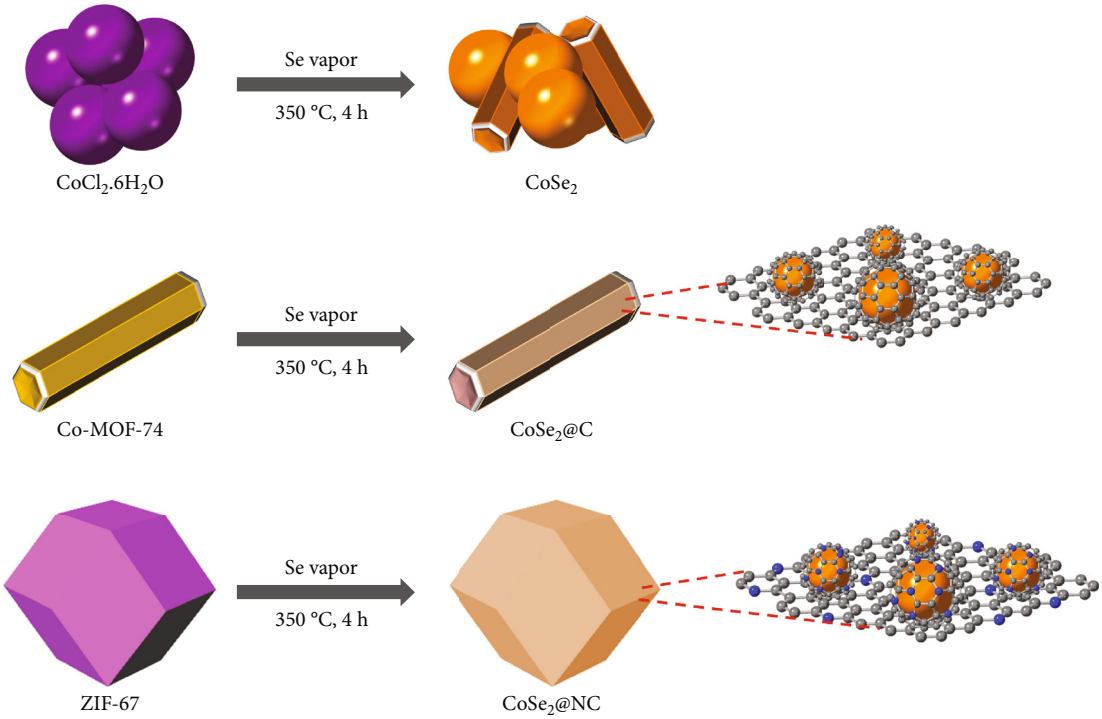

Figure 1: Graphic illustration of the synthesis of $CoSe_2$, $CoSe_2$@C, and $CoSe_2$@NC.

the catalytic activity [23]. As a result, different approaches have been developed to increase the HER catalytic performance of $CoSe_2$. For example, Kong et al. deposited $CoSe_2$ nanograins on carbon cloth as a binder-free and stable electrode for accelerating HER activity [24]. Dai et al. fabricated a hollow $CoSe_2$ structure by means of the Kirkendall effect, which exhibited a low overpotential [25]. Another strategy is to create $CoSe_2$ nanoparticles from cobalt-based metal–organic frameworks (MOFs), which have the advantages of a large surface area, good distribution of metal nodes, and alterable chemical components [26]. For example, Zhou et al. created $CoSe_2$ anchored on carbon nanotubes from a Co-based MOF for accelerating the HER [27]. Although several studies have employed MOFs as sacrificial templates to prepare $CoSe_2$, no study has compared the HER performances of various $CoSe_2$-based materials synthesized from multiple cobalt sources. Besides, Co-based MOF is usually pyrolyzed to form Co metal at relatively high temperatures, followed by selenization technique [28]. This process consumes a lot of energy, and the inheriting of MOF morphology is not well done. For example, Lu et al. pyrolyzed ZIF-67 into Co metal before converting it into $CoSe_2$ nanograin implanted in an N-doped carbon (NC) skeleton for overall water dissociation [29].

In this study, three precursors (ZIF-67, Co-MOF-74, and $CoCl_2.6H_2O$) were used to create $CoSe_2$@NC, $CoSe_2$@C, and $CoSe_2$, respectively, through one-step selenization at low temperature. The $CoSe_2$@NC polyhedrons inherited the regular morphological structure of ZIF-67, which had a larger surface area than $CoSe_2$@C and $CoSe_2$. In addition, nitrogen-doped carbon layers protect the $CoSe_2$ nanograins from electrolyte influences, maintaining their durability after 12 h of operation. As a result, the HER activity of $CoSe_2$@NC is higher than that of $CoSe_2$@C and $CoSe_2$, which is assigned to the integrated strategy of the core–shell architecture and nitrogen-doped carbon, as well as the high surface area. The results of this study prove that using MOFs as precursors is efficient for preparing cobalt selenide electrocatalysts for hydrogen evolution.

2. Experimental

2.1. Chemical and Materials. $Co(NO_3)_2.6H_2O$, $CoCl_2.6H_2O$, 2,5-dihydroxyterephthalic acid (H_4DHBDC), 2-methylimidazole, N, N-dimethylformamide, and 5% Nafion solution were supplied by Sigma-Aldrich. Ethanol and methanol were purchased from Alfa Aesar. Deionized (DI) water was obtained from a Millipore Milli-Q machine.

2.2. Fabrication of ZIF-67 and Co-MOF-74

2.2.1. Fabrication of ZIF-67. 0.718 g of $Co(NO_3)_2.6H_2O$ was stirred in 50 mL of methanol to obtain solution X. Also, 1.622 g of 2-methylimidazole was stirred in 50 mL of methanol to obtain solution Y. Solution X was poured into solution Y under magnetic stirring for 20 h at 25°C. Purple crystals were centrifuged four times with CH_3OH and dried under vacuum at 60°C for 12 h.

2.2.2. Fabrication of Co-MOF-74. First, 0.1 mmol of $Co(NO_3)_2.6H_2O$ and 0.05 mmol of H_4DHBDC acid were added to a mixed solvent containing 3 mL of N, N-dimethylformamide, 3 mL of ethanol, and 3 mL of DI water. The reaction

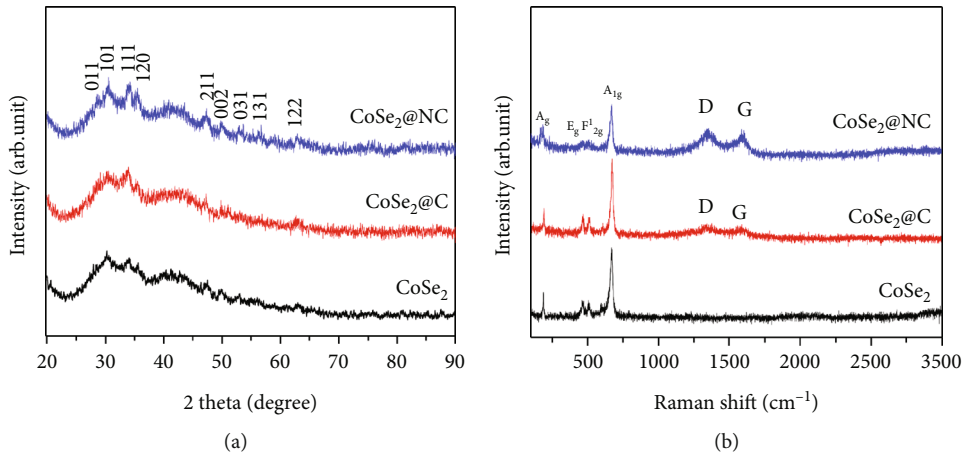

FIGURE 2: (a) Powder XRD patterns of $CoSe_2$ (black line), $CoSe_2$@C (red line), and $CoSe_2$@NC (blue line) and (b) Raman spectra of $CoSe_2$ (black line), $CoSe_2$@C (red line), and $CoSe_2$@NC (blue line).

mixture was then stirred for 30 min and transferred to a glass vial (10 mL) before being placed in a furnace at 100°C. After 24 h, the glass vial is cooled to room temperature, and dark-purple crystals were obtained by centrifugation. These crystals were washed six times with methanol and dried under vacuum at 250°C. The final sample was preserved in vacuum condition.

2.3. Fabrication of $CoSe_2$@NC, $CoSe_2$@C, and $CoSe_2$. Here, 0.1 g each of cobalt-containing sources ZIF-67, Co-MOF-74, and $CoCl_2.6H_2O$ were mixed well with 0.1 g of selenium powder in a crucible and then annealed for 4 h at 350°C to create $CoSe_2$@NC, $CoSe_2$@C, and $CoSe_2$, respectively.

2.4. Material Characterization. The morphological structure of the as-synthesized products was confirmed using scanning electron microscopy (SEM, Carl Zeiss), transmission electron microscopy (TEM, JEOL), and high-resolution TEM. X-ray diffraction (XRD) patterns were recorded using a Bruker D8-Advance device with Cu Kα radiation. Raman spectra of the composites were collected on a LabRAM-HR Evolution with a 532 nm laser. The elemental composition was determined using a K-alpha X-ray photoelectron spectrometry (XPS) system.

2.5. Electrochemical Measurements. The working electrodes were fabricated by coating 5 L of homogeneous suspension onto glassy carbon electrodes (radius of 1.5 mm) with a loading of 0.30 mg cm^{-2}. This suspension was created by sonication of a mixture of 8 mg of material, 0.9 mL of DI water, 1 mL of ethanol, and 0.1 mL of Nafion. The electrochemical HER properties were assessed using a device (Ivium 55630) with a three-electrode system (Pt mesh as the counter electrode and saturated calomel electrode as the reference and working electrode) and 0.5-M H_2SO_4 solution. Polarization plots were reported with IR compensation at a scan rate of 2 mV s^{-1}. Electrochemical impedance spectroscopy was implemented in the frequency mode from 10^5 to 0.1 Hz. Cyclic voltammograms (CVs) utilized for electrochemical double-layer capacitance (C_{dl}) determination were obtained in the nonfaradaic potential region at 25, 50, 75, 100, 125, and 150 mV s^{-1}. The durabilities of the electrocatalysts were compared using chronoamperometric responses (12 h) at specific potentials. The reported voltages were changed to the reversible hydrogen electrode (RHE): $E_{RHE} = E_{SCE} + E^0_{SCE} + 0.059 \times pH$.

3. Results and Discussion

A graphical illustration of the fabrication process is shown in Figure 1. In the synthesis, the $CoSe_2$, $CoSe_2$@C, and $CoSe_2$@NC electrocatalysts were created from $CoCl_2.6H_2O$, Co-MOF-74, and ZIF-67 precursors, respectively, through a selenization process. In the ZIF-67 precursor, $CoSe_2$ nanoparticles were anchored on the N-doped carbon matrix, leading to good dispersion of the active sites. Co-MOF-74 also has $CoSe_2$ nanograins embedded on carbon frameworks, whereas $CoSe_2$ prepared from cobalt chloride does not contain a carbon framework, which could cause the aggregation of nanoparticles. The structural properties of the Co-MOF-74 and ZIF-67 precursors were analyzed using XRD, as shown in Figure S1. The typical peaks are well matched with those reported previously, revealing that Co-MOF-74 and ZIF-67 were successfully prepared [30–34]. The XRD patterns of all samples (Figure 2(a)) can be attributed to orthorhombic $CoSe_2$. The intensive peaks at 28.97°, 30.78°, 34.52°, 35.96°, 47.72°, 50.23°, 53.48°, 56.95°, and 63.29° were indexed in the (011), (101), (111), (120), (211), (002), (031), (131), and (122) planes, respectively [35, 36]. Figure 2(b) shows the Raman spectra of the various cobalt selenide materials. $CoSe_2$@NC and $CoSe_2$@C showed peaks at 1345.5 and 1578.3 cm^{-1}, attributed to the D and G bands of the carbon moieties. In addition, the vibrational frequencies of 174 and 667 cm^{-1} were indexed to the A_g and A_{1g} stretching modes of $CoSe_2$, respectively [27, 35]. More importantly, a high I_D/I_G ratio (1.02) implies that the codoping of Co and N creates rich defects of carbon in $CoSe_2$@NC. They could introduce more active centers of Co-N_x moieties, leading to accelerated HER activity.

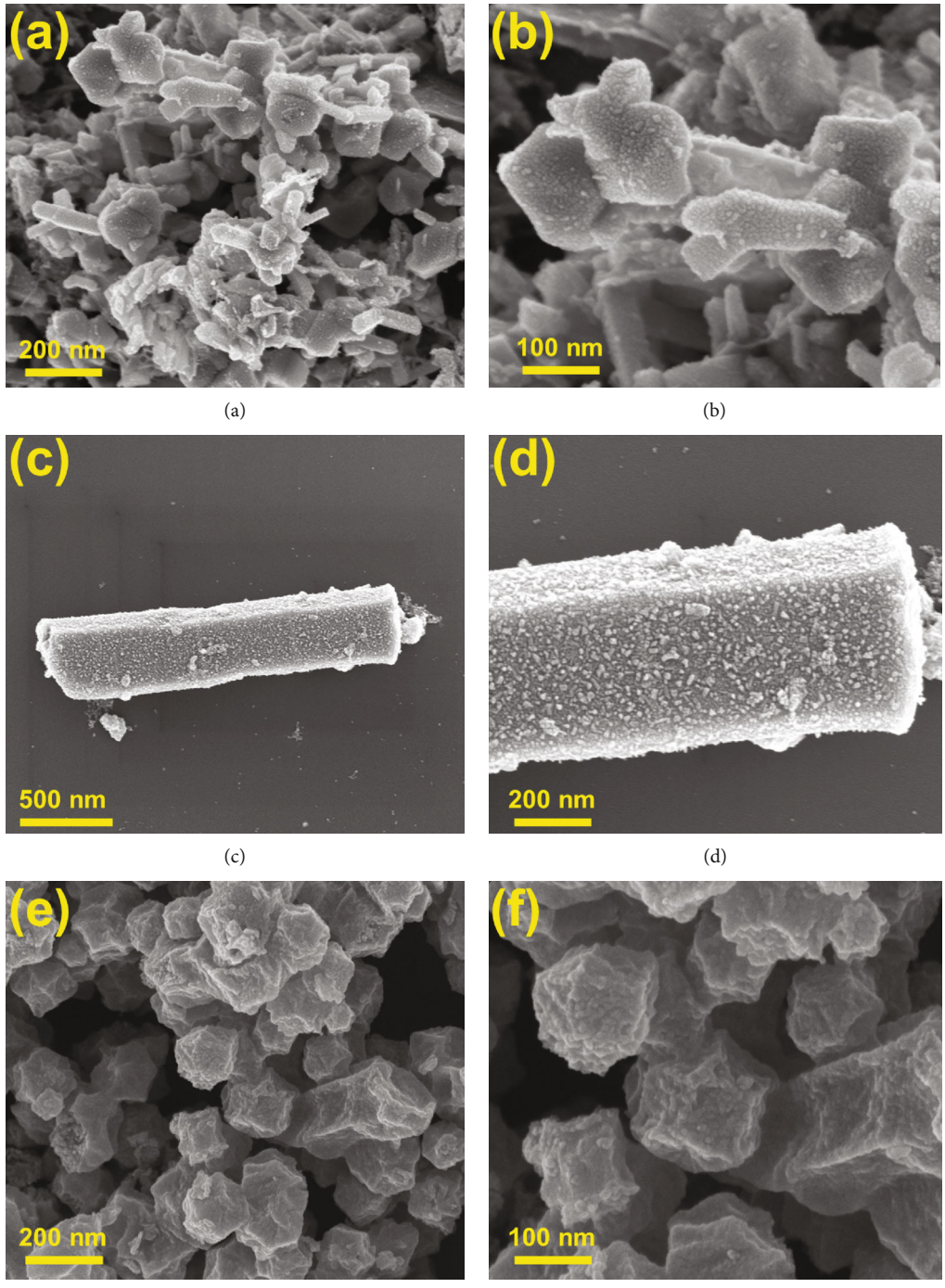

(a) (b) (c) (d) (e) (f)

Figure 3: SEM images of (a, b) $CoSe_2$, (c, d) $CoSe_2$@C, and (e, f) $CoSe_2$@NC.

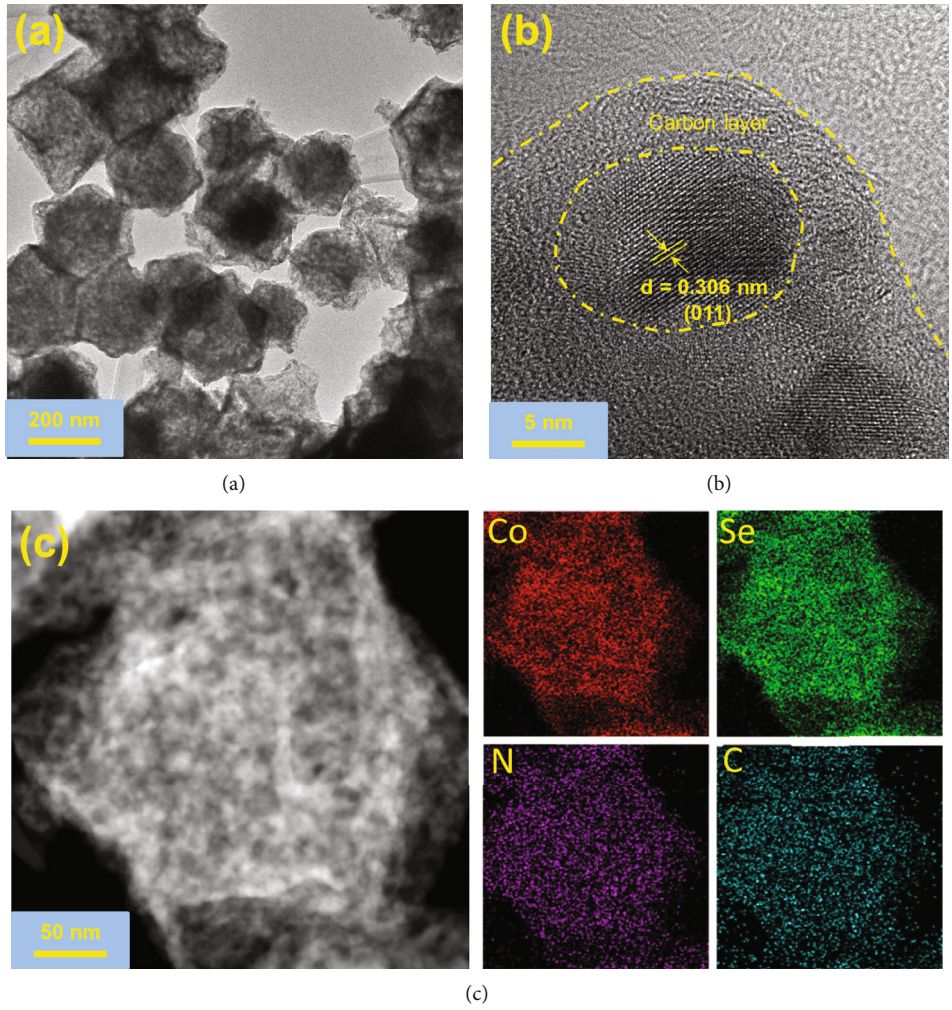

FIGURE 4: (a) TEM images of $CoSe_2$@NC, (b) HR-TEM of $CoSe_2$@NC, and (c) scanning TEM image with elemental mapping of $CoSe_2$@NC.

SEM was utilized to investigate the morphological architectures of various $CoSe_2$ materials. Figures 3(a) and 3(b) show the microsphere structure of $CoSe_2$ with a size of 100 nm, whereas $CoSe_2$@C has a rod-like architecture (Figures 3(c) and 3(d)), identical to Co-MOF-74 (Figure S2a). This phenomenon occurs with $CoSe_2$@NC, which has a polyhedron morphology and a uniform size of 300 nm (Figures 3(e) and 3(f)), inheriting the ZIF-67 structure (Figure S2b). However, the surface of $CoSe_2$@NC is rough and slightly reduced in size. The excellent inheritance of the morphology and porosity of the MOF precursors helped $CoSe_2$@NC (355.2 $m^2 g^{-1}$) and $CoSe_2$@C (129.3 $m^2 g^{-1}$) provide higher BET surface areas than that of $CoSe_2$ (38.7 $m^2 g^{-1}$), as shown in Figure S3. This had beneficial effects on $CoSe_2$@NC in electron/mass transfer [37–39]. TEM and HR-TEM analyses were performed to analyze the morphology of the material further. As shown in Figures 4(a) and 4(b), the $CoSe_2$ nanograins were implanted in N-doped carbon layers to produce a core–shell architecture of $CoSe_2$@NC. In addition, the d-spacing of 0.306 nm was assigned to the (011) plane of $CoSe_2$ (Figure 4(c)). Scanning transmission electron microscopy and elemental mapping show a good distribution of Co, Se, N, and C, as shown in Figure 4(d).

XPS was utilized to analyze the oxidation state and elemental component of $CoSe_2$@NC. The high-resolution XPS spectra of Co 2p in Figure 5(a) show the binding energies of $Co^{2+2}p_{3/2}$ and $Co^{2+2}p_{1/2}$ at 780.6 and 796.9 eV, respectively [23]. Regarding the Se 3d spectra (Figure 5(b)), the binding energies at 55.7 and 54.8 eV are indexed to Se $3d_{3/2}$ and Se $3d_{5/2}$, respectively, indicating the presence of Se_2^{2-} in $CoSe_2$@NC [40]. In addition, a broad peak at 59.2 eV is indexed to SeO_x [41]. The N 1s spectra in Figure 5(c) exhibit peaks at 400.8, 399.5, and 398.4 eV, corresponding to pyrrolic, Co-N_x, and pyridinic [42, 43]. N-doped carbon materials can enhance conductivity, leading to accelerated electrochemical catalytic activity [44–48]. A high-magnification XPS spectrum of C 1s is shown in Figure 5(d). Peaks at 286.3, 285.5, and 284.3 eV are attributed to N-C, -N=C, and C-C [49].

To prove that the use of MOF precursors to fabricate cobalt selenides is efficient in enhancing the HER catalytic activity, the electrochemical properties of $CoSe_2$, $CoSe_2$@C, and $CoSe_2$@NC were analyzed using a three-electrode

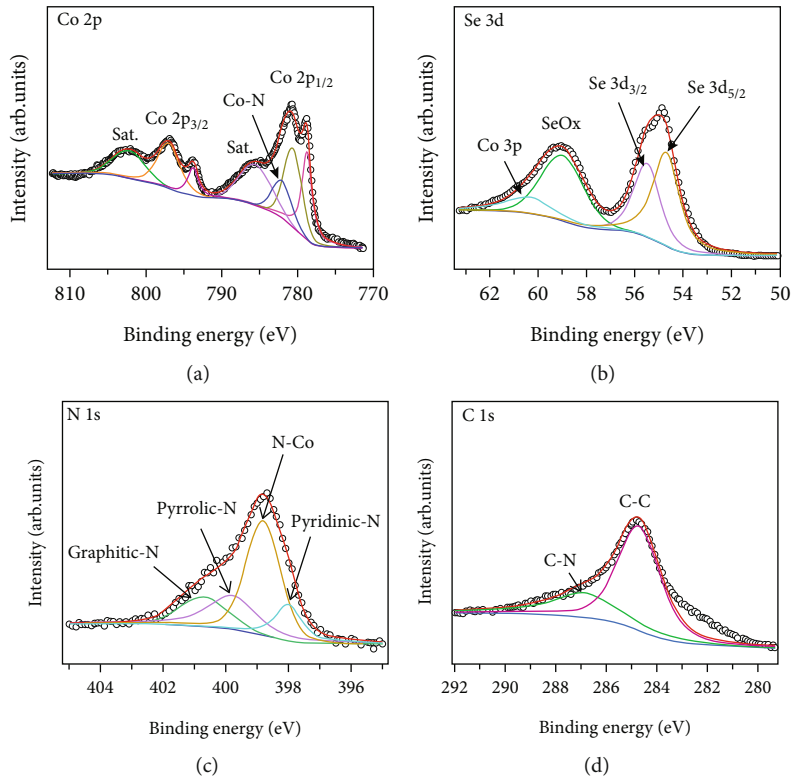

Figure 5: X-ray photoelectron spectra of $CoSe_2$@NC: (a) Co 2p, (b) Se 3d, and (c) N 1s; (d) C 1 s.

system. Figure 6(a) depicts the current–voltage plots of various materials at the same scan rate. The $CoSe_2$@NC sample displayed the lowest overpotential (184 mV), achieving a current density of 10 mA cm^{-2}, indicating better HER catalytic activity than $CoSe_2$@C (220 mV) and $CoSe_2$ (289 mV). The HER performance of $CoSe_2$@NC can be comparable with the other $CoSe_2$-based electrocatalysts (Table S1). Furthermore, $CoSe_2$@NC gives a low Tafel slope of 58.4 mV dec^{-1}, which are smaller values than those of $CoSe_2$@C (71.1 mV dec^{-1}) and $CoSe_2$ (93.6 mV dec^{-1}) (Figure 6(b)). These outcomes indicate that the HER mechanism of $CoSe_2$-based electrocatalysts follows a Volmer–Heyrovesky reaction. Electrochemical impedance spectroscopy was analyzed on $CoSe_2$, $CoSe_2$@C, and $CoSe_2$@NC at a voltage of −0.2 V to confirm the HER kinetics at the electrode–solution interface [50, 51]. As displayed in Figure 6(c), the electron transfer resistance (R_{ct}) of $CoSe_2$@NC (24.5 Ω) is lower than those of $CoSe_2$@C (77.2 Ω) and $CoSe_2$ (149.2 Ω), revealing that N-doped carbon can improve the electron transfer in the HER kinetics of $CoSe_2$@NC. In particular, N-doping creates Co-N_x phases and N-C species, which are favorable for the adsorption of protons to create intermediate H_{ads} and produce H_2 molecules on catalyst surfaces, thus accelerating reaction kinetics [52–54]. Also, the N-doped carbon skeleton facilitates the well-distribution of $CoSe_2$ nanograins and protects them in reaction conditions [28, 55, 56]. This could maximize accessible active centers and enhance the stability of the electrocatalyst. Moreover, the electrochemical surface area (ECSA) was predicted using the double-layer capacitance (C_{dl}) originated from the CV measurements (Figure S4). As displayed in Figure 6(d), the C_{dl} quantity of $CoSe_2$@NC is 3.24 mF cm^{-2}, which is larger than those of $CoSe_2$@C (1.87 mF cm^{-2}) and $CoSe_2$ (1.04 mF cm^{-2}), implying a larger ECSA and more active centers for hydrogen evolution (Table S2).

To compare the intrinsic activities of the electrocatalysts, the turnover frequency (TOF) was determined at the HER overpotential. TOF of cobalt selenide-based electrocatalysts is determined according to a reported formula [57, 58].

$$\mathrm{TOF} = \frac{jA}{nFm}, \tag{1}$$

where j is the current density at a voltage of −200 mV (versus RHE) (A cm^{-2}), A is the geometrical surface area of the working electrode (cm^2), n is the number of electrons transferred to form a molecule of the product (for H_2, it is 2), F is Faraday constant (C mol^{-1}), and m is the number of moles of catalyst coating on the working electrode. As depicted in Figure 7(a), the TOF of $CoSe_2$@NC exhibits a higher TOF of 0.0895 s^{-1}, compared to those of $CoSe_2$@C (0.0197 s^{-1}) and $CoSe_2$ (0.0045 s^{-1}). This implies that $CoSe_2$@NC exhibits a higher performance of the active centers in the electrocatalytic process. Furthermore, the chronoamperometric responses indicated that the as-synthesized $CoSe_2$@NC had excellent stability (Figure 7(b)). $CoSe_2$@NC had approximately 41% of the initial current density, whereas a 76% loss in current density was observed for the $CoSe_2$ catalyst. Also, the decreased current density is attributed to the interference of the hydrogen bubble on the surface of materials. Also, the crystal architecture and morphology of $CoSe_2$@NC did not

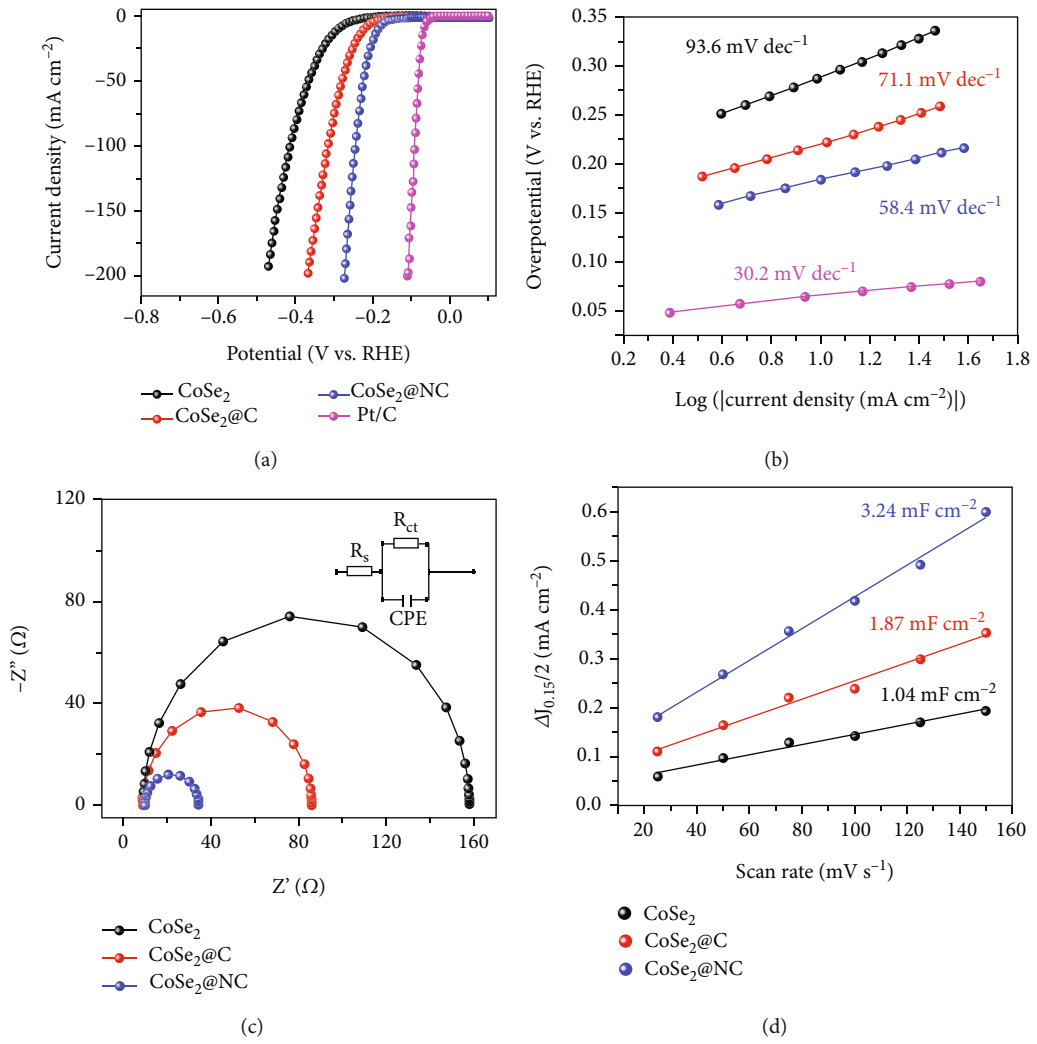

Figure 6: HER performance: (a) polarization plots of $CoSe_2$, $CoSe_2$@C, $CoSe_2$@NC, and Pt/C; (b) Tafel slopes of catalysts; (c) Nyquist plots (recorded with a voltage set at −0.2 V vs. RHE); (d) extracted double-layer capacitances from the CV of different catalysts.

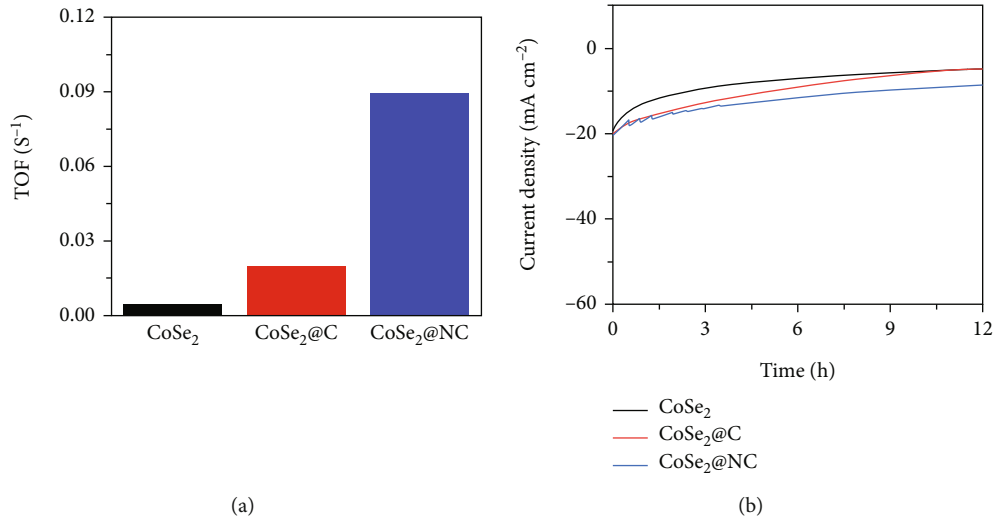

Figure 7: (a) TOFs of $CoSe_2$, $CoSe_2$@C, and $CoSe_2$@NC at an overpotential of 200 mV and (b) chronoamperometric plots of $CoSe_2$, $CoSe_2$@C, and $CoSe_2$@NC at specific potentials for 12 h.

change, which were verified by XRD and SEM after 12 h of testing (Figure S5). The results prove the efficiency of the core–shell structure in improving the stability of the catalysts. Considering the above evaluations, the high HER properties of result $CoSe_2$@NC can be elucidated as follows: (1) the integrating effect of core-shell structure and high surface area of $CoSe_2$@NC allow protecting $CoSe_2$ nanograins, highly exposed active sites, and fast electron transport; (2) N-doping illustrates rich Co-N_x and N-C moieties, good conductivity, and more adsorbed protons, thus accelerating HER performance.

4. Conclusion

The HER catalytic activities of cobalt selenides $CoSe_2$@NC, $CoSe_2$@C, and $CoSe_2$, synthesized using different precursors, were compared. ZIF-67 was used as an N-containing cobalt source to produce the core–shell architecture of $CoSe_2$@NC. The HER performance of $CoSe_2$@NC was higher than those of $CoSe_2$@C and $CoSe_2$, which were generated from Co-MOF-74 and $CoCl_2.6H_2O$, respectively. In particular, $CoSe_2$@NC only required a low overpotential of 184 mV to achieve 10 mA cm^{-2}, whereas the values were 220 and 289 mV for $CoSe_2$@C and $CoSe_2$, respectively. This outcome was assigned to the integrated strategy of the core–shell architecture, rich Co-N_x active centers, and high surface area. In addition, the NC layers protected the $CoSe_2$ nanograins from electrolyte influences, maintaining their durability after 12 h of operation. The results imply that using MOFs as sacrificial templates can efficiently prepare cobalt-selenide-based electrode materials for hydrogen evolution.

Data Availability

The data that support the findings of this study are available from the corresponding authors upon reasonable request.

Conflicts of Interest

The authors declare that they have no conflicts of interest.

Acknowledgments

This research was supported in part by the National Research Foundation of Korea (NRF) (2021R1A4A3027878 and 2022M3H4A1A01012712) and in part by the Korea Agency for Infrastructure Technology Advancement grant (22IFIP-C133622-06) funded by the Ministry of Land, Infrastructure, and Transport. This research was also supported by the Brain Pool Program through the National Research Foundation of Korea (NRF) funded by the Ministry of Science and ICT (grant number 2020H1D3A1A04081409).

Supplementary Materials

Figure S1: XRD patterns of (a) ZIF-67 and (b) Co-MOF-74. Figure S2: FE-SEM images of (a) ZIF-67 and (b) Co-MOF-74. Figure S3: N_2 adsorption–desorption isotherms of $CoSe_2$, $CoSe_2$@C, and $CoSe_2$@NC. Figure S4: cyclic voltammograms (0.1–0.2 V) of (a) $CoSe_2$, (b) $CoSe_2$@C, and (c) $CoSe_2$@NC at various scan rates (25–150 mV s^{-1}) in a 0.5 M H_2SO_4 solution. Figure S5: (a) XRD pattern and (b) SEM images of $CoSe_2$@NC after 12 h of testing. Table S1: comparison of catalytic activity of $CoSe_2$@NC with that of the reported $CoSe_2$-based catalysts for the HER. Table S2: comparison of HER performance of different $CoSe_2$ samples in acidic solution. *(Supplementary Materials)*

References

[1] Y. Z. Wang, M. Yang, Y. M. Ding, N. W. Li, and L. Yu, "Recent advances in complex hollow electrocatalysts for water splitting," *Advanced Functional Materials*, vol. 32, no. 6, article 2108681, 2022.

[2] Z. Zhang, X. Wu, Z. Kou et al., "Rational design of electrospun nanofiber-typed electrocatalysts for water splitting: a review," *Chemical Engineering Journal*, vol. 428, article 131133, 2022.

[3] H. H. Do, Q. V. Le, T. V. Nguyen et al., "Synthesis ofMoSx/Ni-metal-organic framework-74 composites as efficient electrocatalysts for hydrogen evolution reactions," *International Journal of Energy Research*, vol. 45, no. 6, pp. 9638–9647, 2021.

[4] Z. Li, H. Feng, M. Song, C. He, W. Zhuang, and L. Tian, "Advances in CoP electrocatalysts for water splitting," *Materials Today Energy*, vol. 20, article 100698, 2021.

[5] S. J. Patil, N. R. Chodankar, S.-K. Hwang et al., "Co-metal-organic framework derived $CoSe_2$@$MoSe_2$ core-shell structure on carbon cloth as an efficient bifunctional catalyst for overall water splitting," *Chemical Engineering Journal*, vol. 429, article 132379, 2022.

[6] P. M. Pataniya, X. Yang, B. Li, D. Kannichankandy, and C. Sumesh, "Enhanced electrocatalysis ofWSe2nanosheets by partial oxidation for hydrogen generation," *International Journal of Energy Research*, vol. 46, no. 9, pp. 12073–12081, 2022.

[7] T.-G. Woo and I.-S. Park, "Changes in electrical properties of copper-plated layer by organic additives on high current density," *Korean Journal of Metals and Materials*, vol. 58, no. 1, pp. 41–48, 2019.

[8] E. Jo, D. Kim, and J.-Y. Leem, "Facile synthesis of ZnO thin films at low temperatures using an additive-free electrochemical oxidation method," *Korean Journal of Metals and Materials*, vol. 58, no. 9, pp. 645–652, 2020.

[9] D. Kim, T. Lee, and D. Choi, "Optimization of ZnO/cu/ZnO flexible transparent conductive electrodes fabricated by magnetron sputtering," *Korean Journal of Metals and Materials*, vol. 57, no. 12, pp. 795–800, 2019.

[10] F. Davodi, G. Cilpa-Karhu, J. Sainio et al., "Designing of low Pt electrocatalyst through immobilization on support for efficient hydrogen evolution reaction in acidic media," *Journal of Electroanalytical Chemistry*, vol. 896, article 115076, 2021.

[11] J. Zhu, Y. Tu, L. Cai et al., "Defect-assisted anchoring of Pt single atoms on MoS2 nanosheets produces high- performance catalyst for industrial hydrogen evolution reaction," *Small*, vol. 18, no. 4, p. 2104824, 2022.

[12] Y. Chen, R. Ding, J. Li, and J. Liu, "Highly active atomically dispersed platinum-based electrocatalyst for hydrogen evolution reaction achieved by defect anchoring strategy," *Applied Catalysis. B, Environmental*, vol. 301, article 120830, 2022.

[13] H.-Y. Chen, H.-J. Niu, Z. Han, J.-J. Feng, H. Huang, and A.-J. Wang, "Simple fabrication of trimetallic platinum-nickel-cobalt hollow alloyed 3D multipods for highly boosted

hydrogen evolution reaction," *Journal of Colloid and Interface Science*, vol. 570, pp. 205–211, 2020.

[14] Y. Shen, A. C. Lua, J. Xi, and X. Qiu, "Ternary platinum–copper–nickel nanoparticles anchored to hierarchical carbon supports as free-standing hydrogen evolution electrodes," *ACS Applied Materials & Interfaces*, vol. 8, no. 5, pp. 3464–3472, 2016.

[15] A. Hasani, M. Tekalgne, Q. Van Le, H. W. Jang, and S. Y. Kim, "Two-dimensional materials as catalysts for solar fuels: hydrogen evolution reaction and CO2reduction," *Journal of Materials Chemistry A*, vol. 7, no. 2, pp. 430–454, 2019.

[16] G. H. Han, H. Kim, J. Kim, J. Kim, S. Y. Kim, and S. H. Ahn, "Micro-nanoporous MoO_2@CoMo heterostructure catalyst for hydrogen evolution reaction," *Applied Catalysis. B, Environmental*, vol. 270, article 118895, 2020.

[17] R.-L. Zhang, J.-J. Feng, Y.-Q. Yao et al., "Straw-like phosphorus-doped Co_2MnO_4 nanoneedle arrays supported on nickel foam for high-efficiency hydrogen evolution reaction in wide pH range of electrolytes," *Applied Surface Science*, vol. 548, article 149280, 2021.

[18] T. J. Dai, J. Sun, X. S. Peng, J. N. Gong, Z. Y. Zhou, and X. Q. Wang, "In situ synthesis of heterogeneous NiSe2/MoSe2nanocomposite for high-efficiency electrocatalytic hydrogen evolution reaction," *Energy Science & Engineering*, vol. 10, no. 10, pp. 4061–4070, 2022.

[19] S. Liu, X. Lv, G. Liu et al., "In-situ fabrication of Ni_xSe_y/$MoSe_2$ hollow rod array for enhanced catalysts for efficient hydrogen evolution reaction," *Journal of Colloid and Interface Science*, vol. 617, pp. 611–619, 2022.

[20] I. S. Kwon, I. H. Kwak, G. M. Zewdie et al., "WSe2–VSe2alloyed nanosheets to enhance the catalytic performance of hydrogen evolution reaction," *ACS Nano*, vol. 16, no. 8, pp. 12569–12579, 2022.

[21] Z. Liu, D. Gao, L. Hu et al., "Boron-doped $CoSe_2$ nanowires as high-efficient electrocatalyst for hydrogen evolution reaction," *Colloids and Surfaces A: Physicochemical and Engineering Aspects*, vol. 646, article 128903, 2022.

[22] Z. Tian, Y. Liu, Q. Xu et al., "Fe doped $NiSe_2$ nanoarrays to boost electrocatalytic oxygen evolution reaction," *Electrochimica Acta*, vol. 425, article 140711, 2022.

[23] H. Zhang, B. Yang, X. Wu, Z. Li, L. Lei, and X. Zhang, "Polymorphic $CoSe_2$ with mixed orthorhombic and cubic phases for highly efficient hydrogen evolution reaction," *ACS Applied Materials & Interfaces*, vol. 7, no. 3, pp. 1772–1779, 2015.

[24] D. Kong, H. Wang, Z. Lu, and Y. Cui, "$CoSe_2$ nanoparticles grown on carbon fiber paper: an efficient and stable electrocatalyst for hydrogen evolution reaction," *Journal of the American Chemical Society*, vol. 136, no. 13, pp. 4897–4900, 2014.

[25] C. Dai, X. Tian, Y. Nie et al., "Successful synthesis of 3D $CoSe_2$ hollow microspheres with high surface roughness and its excellent performance in catalytic hydrogen evolution reaction," *Chemical Engineering Journal*, vol. 321, pp. 105–112, 2017.

[26] L. Yan, P. Dai, Y. Wang et al., "In situ synthesis strategy for hierarchically porous Ni_2P polyhedrons from MOFs templates with enhanced electrochemical properties for hydrogen evolution," *ACS Applied Materials & Interfaces*, vol. 9, no. 13, pp. 11642–11650, 2017.

[27] W. Zhou, J. Lu, K. Zhou et al., "$CoSe_2$ nanoparticles embedded defective carbon nanotubes derived from MOFs as efficient electrocatalyst for hydrogen evolution reaction," *Nano Energy*, vol. 28, pp. 143–150, 2016.

[28] X. Wang, J. He, B. Yu et al., "$CoSe_2$ nanoparticles embedded MOF-derived Co-N-C nanoflake arrays as efficient and stable electrocatalyst for hydrogen evolution reaction," *Applied Catalysis. B, Environmental*, vol. 258, article 117996, 2019.

[29] H. Lu, Y. Zhang, Y. Huang, C. Zhang, and T. Liu, "Reaction packaging $CoSe_2$ nanoparticles in N-doped carbon polyhedra with bifunctionality for overall water splitting," *ACS Applied Materials & Interfaces*, vol. 11, no. 3, pp. 3372–3381, 2019.

[30] R. Wu, Y. Li, and A. Huang, "Synthesis of high-performance Co-based ZIF-67 membrane for H_2 separation by using cobalt ions chelated PIM-1 as interface layer," *Journal of Membrane Science*, vol. 620, article 118841, 2021.

[31] C. Rösler, A. Aijaz, S. Turner et al., "Hollow Zn/Co zeolitic imidazolate framework (ZIF) and yolk–shell metal@Zn/Co ZIF nanostructures," *Chemistry - A European Journal*, vol. 22, no. 10, pp. 3304–3311, 2016.

[32] A. Zanon, S. Chaemchuen, B. Mousavi, and F. Verpoort, "1 Zn-doped ZIF-67 as catalyst for the CO_2 fixation into cyclic carbonates," *Journal of CO2 Utilization*, vol. 20, pp. 282–291, 2017.

[33] I. Strauss, A. Mundstock, M. Treger et al., "Metal–organic framework Co-MOF-74-based host–guest composites for resistive gas sensing," *ACS Applied Materials & Interfaces*, vol. 11, no. 15, pp. 14175–14181, 2019.

[34] A. de Oliveira, G. F. de Lima, and H. A. De Abreu, "Structural and electronic properties of M-MOF-74 (M = Mg, Co or Mn)," *Chemical Physics Letters*, vol. 691, pp. 283–290, 2018.

[35] C. Miao, X. Xiao, Y. Gong et al., "Facile synthesis of metal–organic framework-derived CoSe2nanoparticles embedded in the N-doped carbon nanosheet array and application for supercapacitors," *ACS Applied Materials & Interfaces*, vol. 12, no. 8, pp. 9365–9375, 2020.

[36] H. Sun, L. Zhang, and Z.-S. Wang, "Single-crystal CoSe2nanorods as an efficient electrocatalyst for dye-sensitized solar cells," *Journal of Materials Chemistry A*, vol. 2, no. 38, pp. 16023–16029, 2014.

[37] L. Moriau, M. Bele, M. Zi et al., "Effect of the morphology of the high-surface-area support on the performance of the oxygen-evolution reaction for iridium nanoparticles," *ACS Catalysis*, vol. 11, no. 2, pp. 670–681, 2021.

[38] B. Liu, S. Xue, S. Tan et al., "Hollow-Co_3O_4@CoP/NS-RGO heterojunction structure derived from ZIF-67 promotes hydrogen evolution reaction and oxygen evolution reaction bifunctional catalysis," *Energy & Fuels*, vol. 36, no. 8, pp. 4532–4540, 2022.

[39] R. Ma, R. Hao, W. Zhou, Y. Cao, and H. Chai, "Hollow CoP microspheres as superior bifunctional electrocatalysts for hydrogen evolution in a broad pH range and oxygen evolution reactions," *Journal of Solid State Chemistry*, vol. 316, p. 123499, 2022.

[40] L. Zhang, Y. Lei, D. Zhou et al., "Interfacial engineering of 3D hollow $CoSe_2$@ultrathin $MoSe_2$ core@shell heterostructure for efficient pH-universal hydrogen evolution reaction," *Nano Research*, vol. 15, no. 4, pp. 2895–2904, 2022.

[41] Y. Zhou, H. Xiao, S. Zhang et al., "Interlayer expanded lamellar $CoSe_2$ on carbon paper as highly efficient and stable overall water splitting electrodes," *Electrochimica Acta*, vol. 241, pp. 106–115, 2017.

[42] X. Zhang, X. Xu, S. Yao et al., "Boosting electrocatalytic activity of single atom catalysts supported on nitrogen-doped carbon through N coordination environment engineering," *Small*, vol. 18, no. 10, article 2105329, 2022.

[43] H. N. Abdelhamid, S. A. Al Kiey, and W. Sharmoukh, "A high-performance hybrid supercapacitor electrode based on ZnO/nitrogen-doped carbon nanohybrid," *Applied Organometallic Chemistry*, vol. 36, no. 1, article e6486, 2022.

[44] Y. J. Sa, S. O. Park, G. Y. Jung et al., "Heterogeneous Co–N/C electrocatalysts with controlled cobalt site densities for the hydrogen evolution reaction: structure–activity correlations and kinetic insights," *ACS Catalysis*, vol. 9, no. 1, pp. 83–97, 2018.

[45] M. Guo, J. Balamurugan, T. D. Thanh, N. H. Kim, and J. H. Lee, "Facile fabrication of Co2CuS4nanoparticle anchored N-doped graphene for high-performance asymmetric supercapacitors," *Journal of Materials Chemistry A*, vol. 4, no. 44, pp. 17560–17571, 2016.

[46] L. Hu, J. Shi, Z. Peng, Z. Zheng, H. Dong, and T. Wang, "A high-density nickel–cobalt alloy embedded in nitrogen-doped carbon nanosheets for the hydrogen evolution reaction," *Nanoscale*, vol. 14, no. 16, pp. 6202–6211, 2022.

[47] W. Zhang, Y.-P. Chen, L. Zhang, J.-J. Feng, X.-S. Li, and A.-J. Wang, "Theophylline-regulated pyrolysis synthesis of nitrogen-doped carbon nanotubes with iron-cobalt nanoparticles for greatly boosting oxygen reduction reaction," *Journal of Colloid and Interface Science*, vol. 626, pp. 653–661, 2022.

[48] J.-J. Duan, R.-L. Zhang, J.-J. Feng, L. Zhang, Q.-L. Zhang, and A.-J. Wang, "Facile synthesis of nanoflower-like phosphorus-doped $Ni_3S_2/CoFe_2O_4$ arrays on nickel foam as a superior electrocatalyst for efficient oxygen evolution reaction," *Journal of Colloid and Interface Science*, vol. 581, pp. 774–782, 2021.

[49] C. He and J. Tao, "Transition metal carbides coupled with nitrogen-doped carbon as efficient and stable bi-functional catalysts for oxygen reduction reaction and hydrogen evolution reaction," *International Journal of Hydrogen Energy*, vol. 47, no. 27, pp. 13240–13250, 2022.

[50] K. Ji, K. Matras-Postolek, R. Shi et al., "MoS_2/CoS_2 heterostructures embedded in N-doped carbon nanosheets towards enhanced hydrogen evolution reaction," *Journal of Alloys and Compounds*, vol. 891, article 161962, 2022.

[51] H. Khan, S. A. Shah, W. Rehman, and F. Chen, "CoS_2 nanoparticles-decorated MoS_2/rGO nanosheets as an efficient electrocatalyst for ultrafast hydrogen evolution," *Advanced Materials Interfaces*, vol. 9, no. 1, article 2101294, 2022.

[52] H. Wang, X. Wang, D. Yang, B. Zheng, and Y. Chen, "$Co_{0.85}Se$ hollow nanospheres anchored on N-doped graphene nanosheets as highly efficient, nonprecious electrocatalyst for hydrogen evolution reaction in both acid and alkaline media," *Journal of Power Sources*, vol. 400, pp. 232–241, 2018.

[53] T. Sun, J. Dong, Y. Huang, W. Ran, J. Chen, and L. Xu, "Highly active and stable electrocatalyst of Ni_2P nanoparticles supported on 3D ordered macro-/mesoporous Co–N-doped carbon for acidic hydrogen evolution reaction," *Journal of Materials Chemistry A*, vol. 6, no. 26, pp. 12751–12758, 2018.

[54] T. Sun, S. Zhang, L. Xu, D. Wang, and Y. Li, "An efficient multifunctional hybrid electrocatalyst: Ni_2P nanoparticles on MOF-derived Co, N-doped porous carbon polyhedrons for oxygen reduction and water splitting," *Chemical Communications*, vol. 54, no. 85, pp. 12101–12104, 2018.

[55] Z. Chen, R. Wu, Y. Liu et al., "Ultrafine Co nanoparticles encapsulated in carbon-nanotubes-grafted graphene sheets as advanced electrocatalysts for the hydrogen evolution reaction," *Advanced Materials*, vol. 30, no. 30, article 1802011, 2018.

[56] Q. Mo, W. Zhang, L. He, X. Yu, and Q. Gao, "Bimetallic $Ni_{2-x}Co_xP$/N-doped carbon nanofibers: solid-solution-alloy engineering toward efficient hydrogen evolution," *Applied Catalysis. B, Environmental*, vol. 244, pp. 620–627, 2019.

[57] N. Srinivasa, J. P. Hughes, P. S. Adarakatti et al., "Facile synthesis of Ni/NiO nanocomposites: the effect of Ni content in NiO upon the oxygen evolution reaction within alkaline media," *RSC Advances*, vol. 11, no. 24, pp. 14654–14664, 2021.

[58] S. Anantharaj, S. Ede, K. Karthick et al., "Precision and correctness in the evaluation of electrocatalytic water splitting: revisiting activity parameters with a critical assessment," *Energy & Environmental Science*, vol. 11, no. 4, pp. 744–771, 2018.